Neuroradiology (2022) 64:1519–1528
https://doi.org/10.1007/s00234-021-02857-x

DIAGNOSTIC NEURORADIOLOGY

Diffusion and perfusion imaging biomarkers of H3 K27M mutation status in diffuse midline gliomas

Nihar Kathrani[1] · Richa Singh Chauhan[2] · Abhishek Kotwal[2] · Karthik Kulanthaivelu[2] · Maya Dattatraya Bhat[2,3] · Jitender Saini[2] · Chandrajit Prasad[2] · Dhritiman Chakrabarti[4] · Vani Santosh[5] · Alok Mohan Uppar[6] · Dwarakanath Srinivas[6]

Received: 20 June 2021 / Accepted: 8 November 2021 / Published online: 27 January 2022

Abstract

Purpose H3K27M-mutant diffuse midline gliomas (M-DMGs) exhibit a clinically aggressive course. We studied diffusion-weighted imaging (DWI) and perfusion (PWI) MRI features of DMG with the hypothesis that DWI-PWI metrics can serve as biomarkers for the prediction of the H3K27M mutation status in DMGs.

Methods A retrospective review of the institutional database (imaging and histopathology) of patients with DMG (July 2016 to July 2020) was performed. Tumoral apparent diffusion coefficient (ADC) and peritumoral ADC (PT ADC) values and their normalized values (nADC and nPT ADC) were computed. Perfusion data were analyzed with manual arterial input function (AIF) and leakage correction (LC) Boxerman-Weiskoff models. Normalized maximum relative CBV (rCBV) was evaluated. Intergroup analysis of the imaging variables was done between M-DMGs and wild-type (WT-DMGs) groups.

Results Ninety-four cases (M-DMGs-$n=48$ (51%) and WT-DMGs-$n=46$(49%)) were included. Significantly lower PT ADC (mutant—1.1 ± 0.33, WT—1.23 ± 0.34; $P=0.033$) and nPT ADC (mutant—1.64 ± 0.48, WT—1.83 ± 0.54; $P=0.040$) were noted in the M-DMGs. The rCBV (mutant—25.17 ± 27.76, WT—13.73 ± 14.83; $P=0.018$) and nrCBV (mutant—3.44 ± 2.16, WT—2.39 ± 1.25; $P=0.049$) were significantly higher in the M-DMGs group. Among thalamic DMGs, the min ADC, PT ADC, and nADC and nPT ADC were lower in M-DMGs while nrCBV (corrected and uncorrected) was significantly higher. Receiver operator characteristic curve analysis demonstrated that PT ADC (cut-off—1.245), nPT ADC (cut-off—1.853), and nrCBV (cut-off—1.83) were significant independent predictors of H3K27M mutational status in DMGs.

Conclusion DWI and PWI features hold value in preoperative prediction of H3K27M-mutation status in DMGs.

Keywords H3K27M · Diffuse midline glioma · MRI

✉ Maya Dattatraya Bhat
mayabhat05@yahoo.co.in

[1] Interventional Radiology, Paras Hospital, Gurugram, Haryana, India

[2] Department of Neuroimaging and Interventional Radiology, National Institute of Mental Health and Neurosciences (NIMHANS), Hosur Road, Near Bangalore Milk Dairy, Karnataka, Bengaluru 5600029, India

[3] Faculty Quarters, NIMHANS, Hosur Road, Near Bangalore Milk Dairy, Karnataka, Bengaluru 5600029, India

[4] Department of Neuroanaesthesia and NeuroCritical Care, National Institute of Mental Health and Neurosciences (NIMHANS), Bengaluru, India

[5] Department of Neuropathology, National Institute of Mental Health and Neurosciences (NIMHANS), Bengaluru, India

[6] Department of Neurosurgery, National Institute of Mental Health and Neurosciences (NIMHANS), Bengaluru, India

Introduction

The year 2012 was a milestone in the expanding knowledge of midline gliomas with the identification of histone gene mutations [1–3]. Diffuse midline glioma (DMG) as an entity of tumors was described for the first time in the WHO classification of CNS tumors 2016 (4). According to cIMPACT-NOW (the Consortium to Inform Molecular and Practical Approaches to CNS Tumor Taxonomy—Not Official WHO) update 2, the entity DMG, H3K27M-mutant should be used only for the tumors that are diffuse, i.e., infiltrating, midline (involving midline structures, e.g., thalamus, brainstem, spinal cord, etc.), gliomas (astrocytic lineage), and are H3K27M mutant [5]. The newly defined entity includes tumors previously denoted as diffuse intrinsic pontine glioma or brainstem glioma along with other gliomas arising

from the thalamus and spinal cord with occasional cases of tumors involving the hypothalamus, ganglio-capsular region, third ventricle, pineal region, cerebellum, and cerebellar peduncles [4, 6–9]. These midline tumors carry a similar recognized mutation (lysine to methionine substitution) at the 27 residues of the N-terminal tail of histone H3 variants, H3.3 (gene H3F3A), and H3.1 (gene HIST1H3B/C) [2, 10]. With the growing awareness of the mutations in the pathway of DMG tumorigenesis (H3 K27, TP53, ACVR1, PDGFRA, EGFR, EZHIP), the newer terminology has been given to the DMGs, i.e., "diffuse midline glioma, H3 K27-altered" in the recent 2021 WHO classification of CNS Tumors [11].

H3K27M-mutant DMGs (M-DMGs) clinically exhibit an aggressive course and display a worse overall prognosis with a short median survival interval of almost 9 to 11 months from the time of diagnosis regardless of the site of the tumor as compared to their wild-type counterparts (WT-DMGs) [2, 12]. Histologically, similar to other gliomas, M-DMGs can also show morphological features of grade II to grade IV gliomas. However, in view of their overall dismal prognosis, they have been classified as WHO grade IV neoplasms, whether or not they fall in the histologically defined category of high-grade tumor [4, 6, 8, 13]. The critical anatomical location and the infiltrative nature of the tumor in the eloquent areas of the brain limit any meaningful surgical resection. Radiotherapy, the current treatment of choice, is largely palliative. No survival benefit has been demonstrated by the adjuvant chemotherapy in prior trials [14]. A biopsy is cautiously refrained as the tumor involves eloquent areas of the brain, underscoring the value of imaging features in the diagnosis of DMG [7, 15]. Most of the studies have reported that DMGs exhibits variable radiologic appearances without distinctive imaging characteristics that could differentiate M-DMGs from WT-DMGs [6, 15–17]. As the occurrence of H3K27M mutation may foresee an aggressive clinical course of the tumor while concurrently giving a prospect for novel targeted treatment methods such as panobinostat and JMJD3, search for the imaging surrogates of these molecular alterations would be useful (6).

Diffusion-weighted imaging (DWI) has been extensively investigated to determine the grade as well as the molecular status (e.g., IDH mutation status) of the gliomas. The tumor cellularity and the aggressiveness of the lesion have been related to the extent of diffusion within and surrounding the tumor (18–21). Dynamic susceptibility contrast perfusion-weighted imaging (DSC-PWI) offers the functional/metabolic information of gliomas non-invasively measuring cerebral hemodynamics at the scale of microcirculation. Apart from its ability to discriminate among grades of the gliomas, it could also predict their progression over time as well as their IDH mutation status (19, 22–25).

To the best of our knowledge, there is only a single study by Chen et al. (2019) that has reported the use of DWI features to differentiate the mutant from WT-DMGs, especially with a limited sample size of 38 cases (19 each, M- and WT-DMGs) (15)(15). Further to this, none of the previous reports has utilized DSC-PWI for the probability assignment of mutational status in the DMGs. We hypothesize that advanced MRI may hold diagnostic value in characterizing DMG and potentially predict mutation status. In this work, we studied the advanced MRI modalities, viz., diffusion and perfusion MRI features of DMG patients retrospectively. Our study aimed at assessing these advanced MRI surrogates to predict the H3K27M mutation status in DMGs non-invasively.

Materials and methods

This retrospective observational study was performed in compliance with the institutional research protocols after institutional research board approval. We retrospectively reviewed our hospital's database of patients with DMG from July 2016 to July 2020.

Patient cohort

The patients included in the study had MRI suggestive of DMG, involving various midline structures of the brain, including the septal region, thalamus, brainstem, cerebellum, middle cerebellar peduncles, and pineal region. These were patients in whom MRI was performed before any biopsy, surgical resection, or the initiation of other kinds of therapy. The intervention was executed within one month of the MRI examination. Patients with hemispheric and spinal cord gliomas, biopsy-proven WHO grade I pilocytic astrocytomas, non-glioma tumor subtypes, and inconclusive biopsy were excluded from the study. Biopsy-proven DMG cases with MRI study of poor diagnostic quality were excluded. A total of 94 cases satisfied the inclusion criteria, of which 48 patients had M-DMGs, and 46 patients had WT-DMGs (Fig. 1).

Histopathology and immunohistochemistry

Surgical resection had been performed in 71 of 94 patients, and 23 patients underwent stereotactic biopsy. The Neuropathologist had reviewed all the tumors and categorized them as phenotypic low-grade diffuse astrocytomas (grade II), anaplastic astrocytomas (grade III), glioblastomas (GBM) (grade IV), and diffuse midline gliomas-H3K27M-mutant (grade IV). The formalin-fixed paraffin-embedded Sects. (4 μm) from the blocks had been collected on silane-coated slides, and the VENTANA BenchMark automated staining system (VENTANA BenchMark-XT) was used for immunohistochemistry (IHC). For a short time, the sections

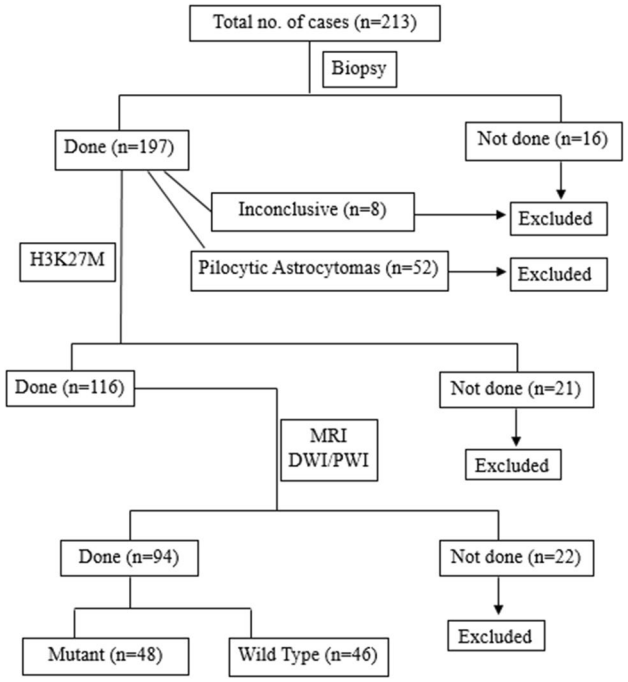

Fig. 1 Inclusion and exclusion criteria. Flow diagram depicting the selection process and cases included in the study (*n*, number of patients)

had been subjected to antigen retrieval and subsequently incubated with primary and secondary antibodies. Hematoxylin was used for counterstaining. The antibody used was H3K27me3 (Millipore, 07–449; 1:100) (H3.3K27Mme3, Malaysia, RM192, 1:100) with appropriate positive or negative controls incorporated in each batch of staining.

Image acquisition

MRI scans had been performed on the 1.5 (Aera 1.5 T, Siemens Medical Systems, Erlangen, Germany) or 3.0 (Achieva 3 T, Philips Medical Systems, Best, Netherlands) Tesla MR scanners using 32-channel head coil as per standard operating procedure with/without sedation. MRI protocol for the diffusion and perfusion data acquisition included the following sequences: diffusion tensor imaging in the axial plane (oriented along anterior commissure-posterior commissure line) with a spin echo-planar sequence (6 directions, TR/TE: 2424/72 ms, section thickness = 4 mm, intersection thickness = 1 mm, NEX 1.0, matrix size 230 × 230, *b*-values: 0 and 1000 s/mm^2 with diffusion gradients encoded in six orthogonal directions to generate 3 sets of diffusion-weighted maps, i.e., the isotropic trace DW, ADC, and FA maps). DSC-PWI was a single-shot gradient-recalled T2*-weighted echo-planar imaging sequence [EPI factor: 41, flip angle: 75°, TR/TE: 1606/40 ms, section thickness: 4 mm, intersection thickness: 1 mm, NEX:1.0, FOV: 220 × 220 mm]. For DSC perfusion, during the first 7 phases, images had been acquired before injecting the contrast material to establish a pre-contrast baseline. In the 8th phase, gadopentetate dimeglumine in a dose of 0.1 mmol/kg body weight and 5 ml/s injection rate was injected intravenously with an MRI-compatible power injector, followed by 20-ml saline chase at the same injection rate. Then, a series of 40 dynamics, comprising of 1200 images (30 sections) were obtained in 1 min 9 s.

Image analysis

The MR diffusion and raw perfusion data were digitally transferred from the picture archiving and communication system to and processed in Philips IntelliSpace Portal (ISP) software version 9.0. Diffusion data of some of the cases were analyzed on the SIEMENS workstation additionally.

For tumor, apparent diffusion coefficient (ADC) values and multiple ROIs of 10–20 mm^2 (as per an earlier study by Darbar et al. (26)) were drawn on the ADC maps, and the ROI with the lowest mean value was taken (min ADC) and normalized with the contralateral normal-appearing posterior limb of the internal capsule (PLIC) to get the normalized ADC (nADC). The lowest value was chosen for ADC as it has been observed to show the highest accuracy for distinguishing tumor grade and has been used in various previous studies owing to a better interobserver agreement (26, 27). The ROIs were placed in the solid portions of the tumor, avoiding obvious areas of necrosis, cysts, hemorrhage, or blood vessels which might influence the ADC values. For peritumoral ADC (PT ADC) values, ROIs were placed in the peritumoral T2/FLAIR hyperintense signal, or within 1 cm of the tumor margin, for cases without peritumoral hyperintensity. The PT ADC was also normalized with the contralateral normal PLIC (nPT ADC) (Fig. 2). ADC was expressed in mm^2/s.

For interpretation of the perfusion data, whole-brain rCBV maps were generated by applying a single compartmental model with manual arterial input function (AIF) as well as leakage correction (LC) Boxerman-Weiskoff model (28). Either of the middle cerebral arteries was selected for manual AIF analysis. Multiple ROIs of dimensions of approximately 30–40 mm^2 were drawn on the enhancing/diffusion restricted/homogeneous aspect of the tumor. The ROI size was chosen as per our departmental protocol and in accordance with the previous studies (29, 30). The maximum relative CBV (rCBV; as determined by the manual AIF method and expressed as milliliters of blood per 100 g of brain tissue) and leakage-corrected and leakage-uncorrected rCBV (as determined by the LC method) of the tumor ROI were extracted. The maximum rCBV values were selected for quantitative analysis as this approach has been shown to provide the best interobserver and intraobserver

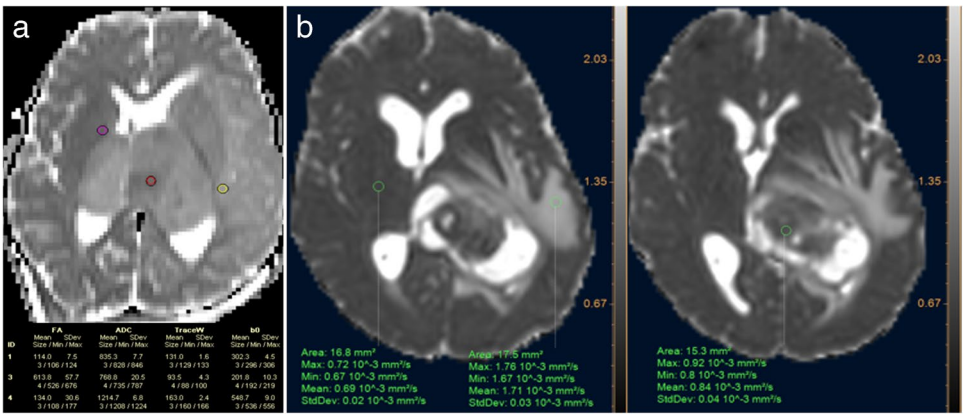

Fig. 2 **a** and **b** depict the placement of tumoral, peritumoral, and internal capsule diffusion ROIs in Siemens workstation (**a**) and Philips ISP (**b**)

reproducibility in previous studies (31, 32). Normalization of the rCBV was performed by calculating ratio of maximum tumor rCBV to the maximum CBV of the contralateral unaffected white matter (nrCBV/ uncorrected nrCBV) to minimize the interindividual/inter-scanner variation in rCBV values (Fig. 3). Similarly, normalized values of tumoral rCBF (cerebral blood flow), corrected rCBV, and K2 values were also calculated. K2 is a permeability-weighted leakage coefficient, derived from the LC model which can be considered an imaging biomarker of microvascular permeability (leakiness) (28).

Intergroup analysis of the imaging variables parameters was done between M- and WT-DMG groups, irrespective of tumor grade and location. Furthermore, subgroup analysis for location (thalamic/brainstem) and grade IV M-DMGs and WT-DMGs was also performed.

Statistical analysis

Data was collated offline in a Microsoft Excel 2007 spreadsheet in a de-identified manner and was analyzed using R software version 3.5.2. Interval scale data were presented

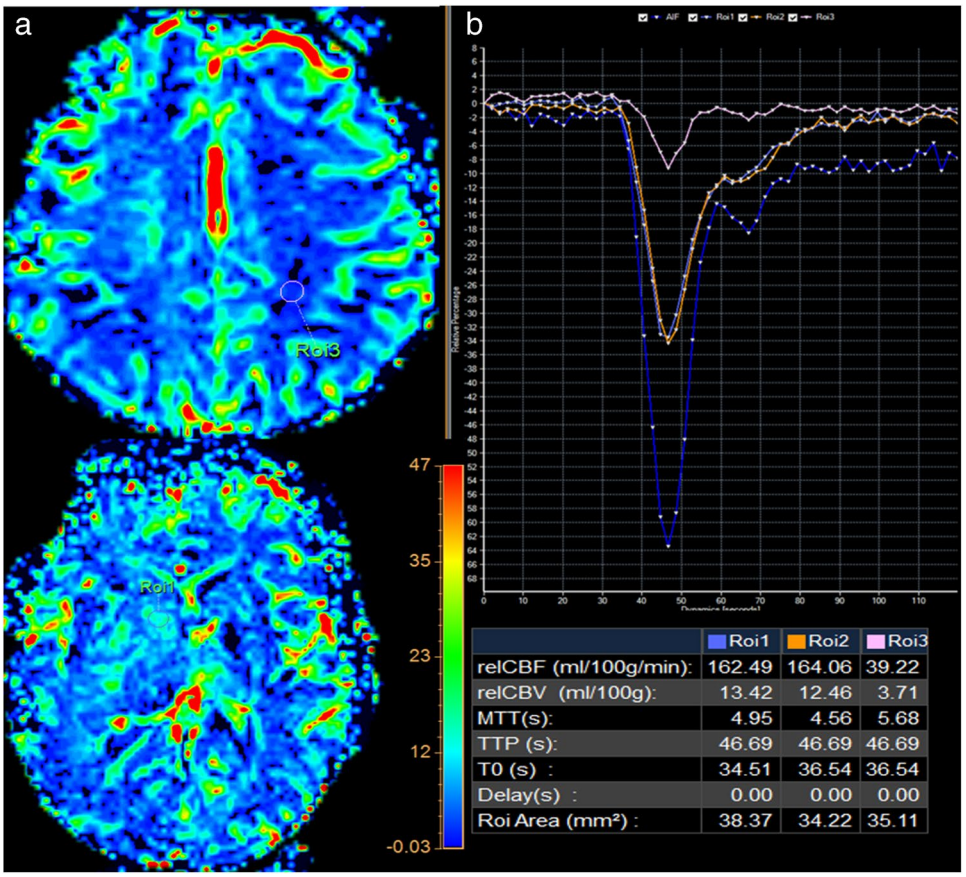

Fig. 3 **a** shows the placement of ROIs for the tumor perfusion analysis in the normal-appearing white matter and the tumor. **b** depicts the perfusion curve and the derived values of various perfusion parameters

as means and standard deviations, and nominal scale data as frequencies and percentages. Between-group analysis of interval scale data was conducted using non-parametric Mann–Whitney *U* test and of nominal scale data, using chi-square test with or without Yate's correction. For finding cut-off of interval scale variable levels to predict histone mutation status, receiver operating characteristic (ROC) curve analysis was conducted, and the best cut-off was found using Youden's method. In case of conflict of multiple levels being found by Youden's method, higher specificity of prediction was used as the benchmark for appropriate level selection. $P < 0.05$ was considered statistically significant.

Results

Forty-eight (51%) out of the 94 cases were M-DMG (21 males/27 females), while 46 patients (49%) had WT-DMGs (27 males/19 females). The mean age of patients in the M-DMG group was 23.04 ± 13.74 years, while in the WT group was 33.83 ± 18.55 years ($P = 0.0000007$). The gender distribution was not significantly different between the two groups. In our study, the majority of the tumors were located in the thalamus (60%), followed by the brainstem (25%) and other locations (15%; cerebellum, middle cerebellar peduncles, pineal region, and septum pellucidum). The majority of the brainstem gliomas (18/24) were mutation-positive ($P = 0.001$) (Table 1). Perfusion data were available in 64 cases, out of which 34 cases were M-DMG.

Significantly lower PT ADC (mutant—1.1 ± 0.33, WT—1.23 ± 0.34; $P = 0.033$) and nPT ADC (mutant—1.64 ± 0.48, WT—1.83 ± 0.54; $P = 0.040$) were noted in the M-DMGs. Among the various perfusion parameters evaluated, the rCBV (mutant—25.17 ± 27.76, WT—13.73 ± 14.83; $P = 0.018$), nrCBV (mutant—3.44 ± 2.16, WT—2.39 ± 1.25; $P = 0.049$), rCBF (mutant—266.15 ± 189.26, WT—181.91 ± 167.97; $P = 0.017$), and uncorrected nrCBV (mutant—3.5 ± 2.05, WT—2.54 ± 1.56; $P = 0.019$) were statistically different between the two groups, being significantly higher for the M-DMG group (Figs. 4 and 5).

Within the subgroup of thalamic tumors, both the min ADC (mutant—0.76 ± 0.18, WT—0.89 ± 0.24; $P = 0.042$) and PT ADC (mutant—1.19 ± 0.37, WT—1.3 ± 0.38; $P = 0.050$) as well as the nADC (mutant—1.11 ± 0.27, WT—1.31 ± 0.36; $P = 0.036$) and nPT ADC (mutant—1.74 ± 0.53, WT—1.93 ± 0.57; $P = 0.049$) showed a significant difference, being lower for the M-DMGs than the WT-DMGs. Among the perfusion parameters of the thalamic tumors, the nrCBV ($P = 0.043$), rCBF ($P = 0.021$), nrCBF ($P = 0.013$), uncorrected rCBV ($P = 0.009$), uncorrected nrCBV ($P = 0.008$), and corrected rCBV ($P = 0.06$) showed significant difference, the variables being significantly higher for the M-DMGs (Figs. 4, 5, and 6) (online resource).

No intergroup differences were noted in the analyzed variables within the subgroup of brainstem DMGs. Furthermore, we did not find any significant difference in the values of FA on DWI and K2 on PWI between the groups (online resource).

ROC curve analysis

We validated our results with the ROC curve analysis. It showed that the PT ADC (cut-off—1.245; AUC 0.627) and nPT ADC (cut-off—1.853; AUC—0.623) were significant independent predictors of H3K27M mutational status in DMGs. In thalamic subgroup nADC (cut-off—1.129; AUC—0.664), PT ADC (cut-off—1.185; AUC—0.651), and nPT ADC (cut-off—1.853; AUC—0.653) demonstrated a significant independent predictive value for H3K27M mutational status (Fig. 4, Table 2).

Similarly, nrCBV (cut-off—1.83; AUC—0.645) and uncorrected nrCBV (cut-off—2.28; AUC—0.673) could independently discriminate the M- and WT-DMGs with optimal sensitivity and specificity. Among the thalamic

Table 1 Patients' demographic data and location of the mutant and WT DMGs

	All patients ($n = 94$)	H3K27M mutant ($n = 48$)	H3K27M WT ($n = 46$)
Age range (in years)	2–70	3–55	2–70
Mean ± SD	28.32 ± 17.07	23.04 ± 13.74	33.83 ± 18.55
Gender			
Male	48	21	27
Female	46	27	19
Location (*n* (%))			
Thalamus	56 (60)	28 (58)	28 (61)
Midbrain	8 (8)	6 (12.5)	2 (4)
Pons	13 (14)	10 (21)	3 (7)
Medulla	3 (3)	2 (4)	1 (2)
Others	14 (15)	2 (4)	12 (26)

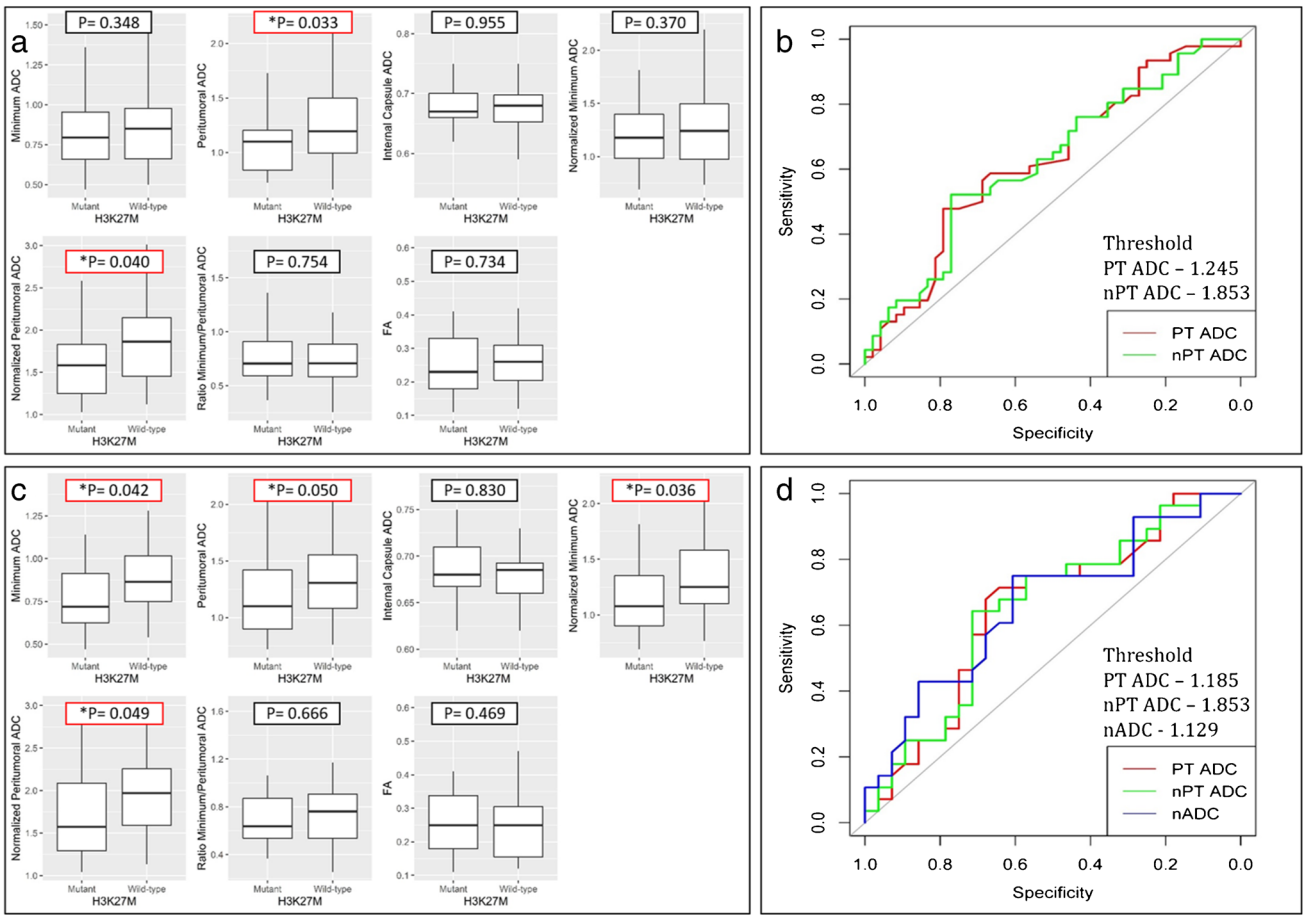

Fig. 4 **a** and **c** depict the box plots of the distribution of the various diffusion parameters of the tumor, internal capsule, and peritumoral region between the H3 K27M-mutant and WT groups and thalamic subgroup respectively. **b** and **d** represent the ROC curves for the significantly different diffusion parameters between the overall M- and WT-DMGs and between the thalamic subgroup respectively

tumors, nrCBV (cut-off—1.83; AUC—0.703), nrCBF (cut-off—2.73; AUC—0.738), and uncorrected nrCBV (cut-off—2.27; AUC—0.759) demonstrated a significant independent predictive value for H3K27M mutational status (Fig. 5, Table 3).

Discussion

We observed that the peritumoral region of M-DMGs exhibited lower ADC values than those of the WT-DMGs. This, at least in part, indicates higher cell density in the peritumoral area of the M-DMGs. However, the tumor ADC values were not significantly different between the M- and WT-DMGs. This is in contrast to observations of Chen et. al., who have reported that both the minimal tumor ADC and PT ADC of the M-DMGs were significantly lower than the WT-DMGs (15). On subgroup analysis of thalamic tumors, we observed that both the minimal tumor and PT ADC, as well as the normalized tumor and PT ADC, were significantly lower for the M-DMGs than the WT-DMGs, while no such difference was evident when analyzed for brainstem DMGs alone. This location ought to be contextualized for the discordance of our findings with those of Chen et al. as well, wherein the majority of the M-DMGs ($n = 12/19$, 63.2%) were thalamic while only 15.8% ($n = 3/19$) were brainstem tumors (15). The difference in the number of brainstem gliomas in our study could possibly have skewed the diffusion results. This again represents the significance of the effect of location on the intrinsic characteristics of the DMGs. Between grade IV M- and WT-DMGs, PT ADC and nPT ADC of WT-DMGs were found to be significantly higher than that of M-DMGs. The greater cellular proliferation and surrounding parenchymal infiltration by the tumor cells in M-DMGs than their WT counterparts could be a possible explanation for this finding; both the tumors being matched in their high-grade histomorphology.

The present study also revealed that the rCBV ratio (or nrCBV) and uncorrected rCBV ratio (or uncorrected nrCBV) were significant independent variables correlating to the

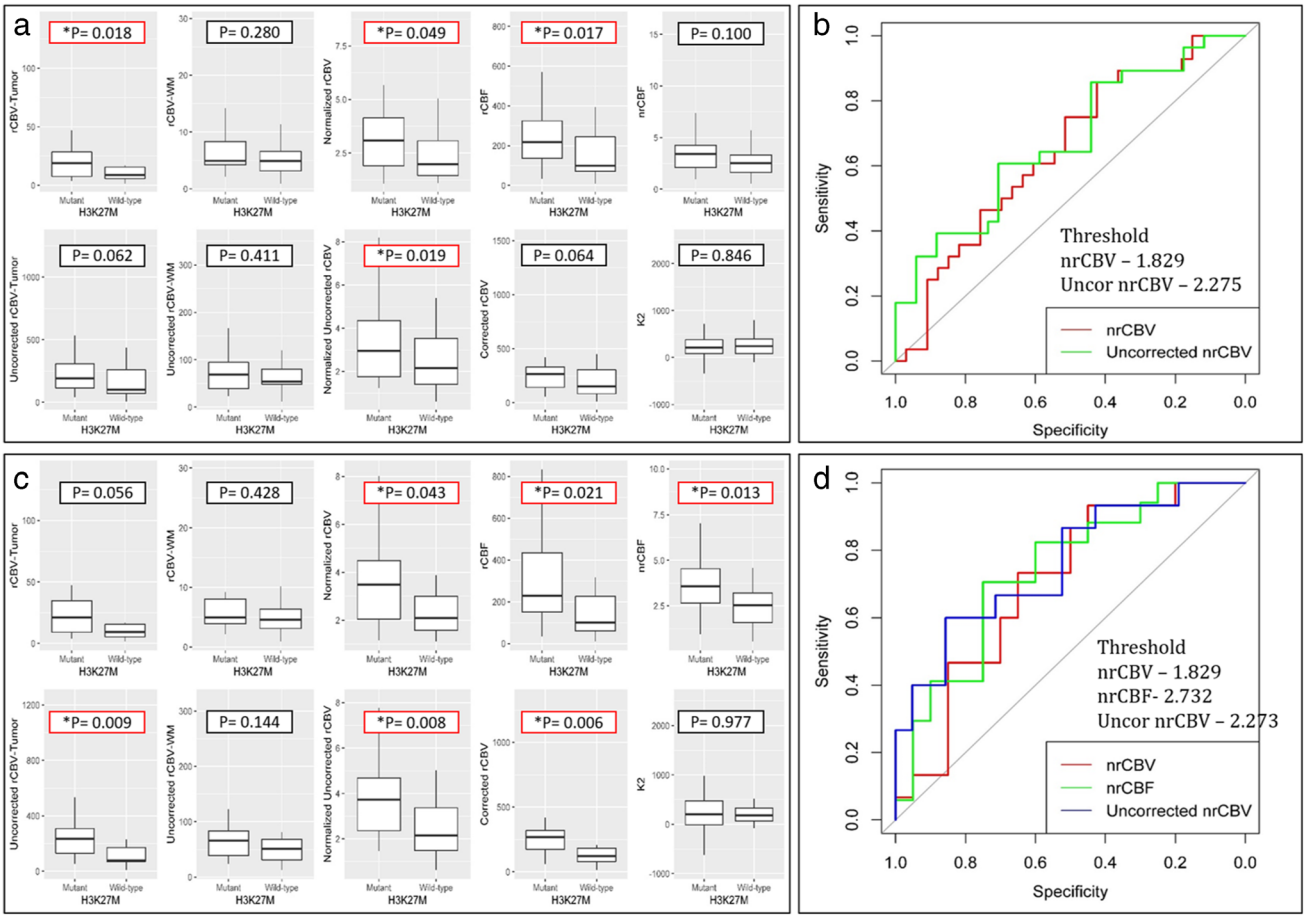

Fig. 5 **a** and **c** depict the box plots of the distribution of the various perfusion parameters of the tumor and normal-appearing white matter between the H3 K27M-mutant and WT groups and thalamic subgroup respectively. **b** and **d** represent the ROC curves for the significantly different perfusion parameters between the overall M- and WT-DMGs and between the thalamic subgroup respectively

histone mutation status in DMGs. Both these parameters were significantly high ($P = 0.049$ and 0.019 respectively) in the mutant as compared to the WT-DMGs. Thalamic M- and WT-DMGs exhibited significant differences in terms of nrCBF and corrected rCBV also, in addition to the nrCBV and uncorrected nrCBV. These parameters with optimal sensitivity and specificity can serve as biomarkers of the mutational status of DMGs (Table 3). The H3K27M mutation drives the overexpression of growth factors like PDGF and VEGF due to amplification and recurrent mutations of signaling genes like ACVR1, PI3K, and RTKs. These later mutations promote neoangiogenesis (33, 34), which could be the possible reason for the M-DMGs being perfused higher than the WT-DMGs as witnessed in this study. Piccardo et al. also observed in their study that on comparing the mutant and WT-DMGs (irrespective of the tumor histologic grade), the arterial spin labeling (ASL)–derived rCBF was higher in the M-DMGs (35). The lack of intergroup difference in the perfusion results in the brainstem DMGs could indicate that the influence of this mutation in different anatomical locations may be variable, and these tumor subsets can be studied in a more comprehensive manner.

Our study has some general and study-specific limitations. Firstly, there was a lack of clinical follow-up data regarding the survival and prognosis of the patients. Secondly, we did not perform subgrouping of the histone of the H3.3/H3.1 gene group that could have been interesting. Thirdly, the data were acquired on two scanners with different field strengths. Previous reports (36–38) had suggested that the ADC values were comparable in gliomas as well as in head and neck cancers when measured using 1.5-T and 3-T scanners. Their results led us to compare our results among different field strengths. We have tried to address this limitation by normalizing the DWI and PWI parameters with the uninvolved white matter structures; however, we acknowledge that this factor might have an impact on the generalizability of the results. Lastly, it was a single-institution retrospective study. Future studies with more extensive clinical data are needed to establish the generalizability of the results and recognize various other aspects

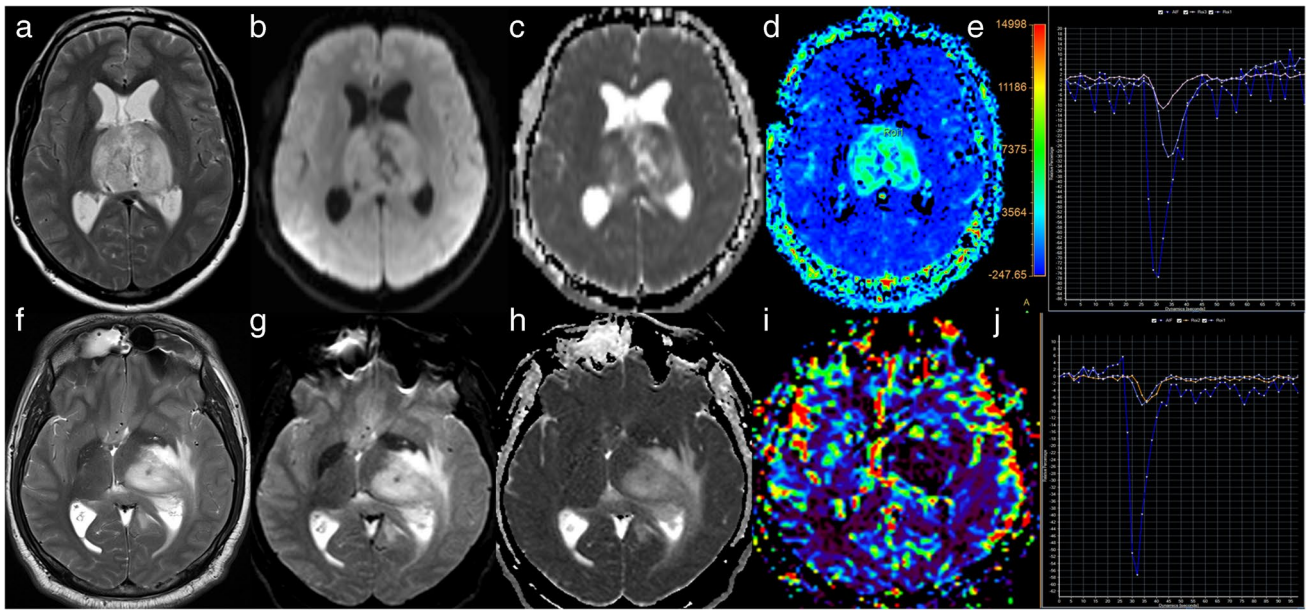

Fig. 6 Examples of H3K27M-mutant and wild-type DMGs. **a–e** A 32-year male with bithalamic H3K27M-mutant DMG shows a well-defined, heterogeneously T2 hyperintense tumor. DWI with ADC map shows striking diffusion restriction within the tumor. rCBV map and the curve of the DSC-PWI show that the tumor is markedly hyper-perfused. **f–j** A 43-year male with left thalamic H3 K27M WT-DMG depicts a poorly marginated T2 hyperintense tumor with associated perilesional edema. DWI with ADC map shows no diffusion restriction within the tumor. rCBV map and the curve of the DSC-PWI show that the tumor is hypoperfused

Table 2 Measurement of cut-off, specificity, sensitivity, and AUC of DWI parameters for assessing the H3 K27M status (overall and thalamic subgroup)

Parameters	Cut-off/threshold	95% confidence interval		Specificity (%)	Sensitivity (%)	AUC (95%CI)
		Lower bound	Upper bound			
Overall						
PT ADC	1.245	0.514	0.741	79.2	47.8	0.627
nPT ADC	1.853	0.510	0.737	77.1	52.2	0.623
Thalamic						
nADC	1.129	0.520	0.808	75.0	60.7	0.664
PT ADC	1.185	0.502	0.799	67.9	67.9	0.651
nPT ADC	1.853	0.506	0.800	71.4	64.3	0.653

Table 3 Measurement of cut-off, specificity, sensitivity, and AUC of DSC-PWI parameters for assessing the H3 K27M status (overall and thalamic subgroup)

Parameters	Cut-off/threshold	95% confidence interval		Specificity (%)	Sensitivity (%)	AUC (95%CI)
		Lower bound	Upper bound			
Overall						
nrCBV	1.829	0.505	0.785	75.8	46.4	0.645
Uncorrected nrCBV	2.275	0.537	0.809	70.6	60.7	0.673
Thalamic						
nrCBV	1.829	0.527	0.880	85	46.7	0.703
nrCBF	2.732	0.575	0.902	75	70.6	0.738
Uncorrected nrCBV	2.273	0.596	0.921	85.7	60	0.759

of M-DMGs, like outcome and management strategies, which are not discussed in this paper.

Conclusion

This work, a first of its kind, has explored the diagnostic utility of advanced MRI modalities, viz., perfusion MRI and diffusion MRI in patients with M- and WT-DMGs. The diffusion MRI features (tumor and PT ADC and normalized tumor and nPT ADC) and perfusion MRI features (normalized rCBV, rCBF, and uncorrected rCBV) can potentially discriminate between the M-DMGs and WT-DMGs. The diffusion within the tumor as well as the PT region of the M-DMGs is lower as compared to the WT-DMGs, and the M-DMGs are markedly hyper-perfused as compared to the WT-DMGs. Larger studies are, however, needed to further investigate these results.

Supplementary Information The online version contains supplementary material available at https://doi.org/10.1007/s00234-021-02857-x.

Authors' contributions All authors contributed to the study conception and design. Material preparation, data collection, and analysis were performed by Richa Singh Chauhan, Karthik Kulanthaivelu, Abhishek Kotwal, and Maya Dattatraya Bhat. The first draft of the manuscript was written by Nihar Kathrani and Richa Singh Chauhan and all authors commented on previous versions of the manuscript. All authors read and approved the final manuscript.

Funding No funding was received for conducting this study.

Declarations

Conflicts of interest The authors have no conflicts of interest to declare that are relevant to the content of this article.

Ethics approval This retrospective study involving human participants was in accordance with the ethical standards of the institutional and national research committee and with the 1964 Helsinki Declaration and its later amendments or comparable ethical standards. The Human Investigation Committee (IRB) of the National Institute of Mental Health and Neurosciences, Bengaluru, India, approved this study.

Consent to participate Informed consent was waived off from participants owing to its retrospective nature.

Consent for publication Patients consent was waived off owing to the retrospective nature of the study.

Availability of data and material Complete research data will be available whenever requested.

Code availability Not applicable.

References

1. Alelú-Paz R, Ashour N, González-Corpas A, Ropero S (2012) DNA methylation, histone modifications, and signal transduction pathways: a close relationship in malignant gliomas pathophysiology. J Signal Transduct 2012:1–8
2. Khuong-Quang DA, Buczkowicz P, Rakopoulos P, Liu XY, Fontebasso AM, Bouffet E et al (2012) K27M mutation in histone H3.3 defines clinically and biologically distinct subgroups of pediatric diffuse intrinsic pontine gliomas. Acta Neuropathol. 124(3):439–47
3. Schwartzentruber J, Korshunov A, Liu XY, Jones DT, Pfaff E, Jacob K et al. Driver mutations in histone H3.3 and chromatin remodelling genes in paediatric glioblastoma. Nature 482:226–31. https://doi.org/10.1038/nature10833
4. Louis DN, Perry A, Reifenberger G, von Deimling A, Figarella-Branger D, Cavenee WK et al (2016) The 2016 World Health Organization classification of tumors of the central nervous system: a summary. Acta Neuropathol 131(6):803–820
5. Louis DN, Giannini C, Capper D, Paulus W, Figarella-Branger D, Lopes MB et al (2018) cIMPACT-NOW update 2: diagnostic clarifications for diffuse midline glioma, H3 K27M-mutant and diffuse astrocytoma/anaplastic astrocytoma, IDH-mutant. Acta Neuropathol. 135(4):639–42. https://doi.org/10.1007/s00401-018-1826-y
6. Daoud EV, Rajaram V, Cai C, Oberle RJ, Martin GR, Raisanen JM et al (2018) Adult brainstem gliomas with H3K27M mutation: radiology, pathology, and prognosis. J Neuropathol Exp Neurol 77(4):302–311
7. Johnson DR, Guerin JB, Giannini C, Morris JM, Eckel LJ, Kaufmann TJ (2017) 2016 updates to the WHO brain tumor classification system: what the radiologist needs to know. Radiographics 37(7):2164–2180
8. Louis DN, Ohgaki H, Wiestler OD, Cavenee WK, Ellison DW, Figarella-Branger D, et al. The 2016 WHO classification of tumors of the central nervous system. International Agency for Research on Cancer (IARC), Lyon. 2016.
9. Solomon DA, Wood MD, Tihan T, Bollen AW, Gupta N, Phillips JJJ et al (2016) Diffuse midline gliomas with histone H3–K27M mutation: a series of 47 cases assessing the spectrum of morphologic variation and associated genetic alterations. Brain Pathol 26(5):569–580
10. Lu QR, Qian L, Zhou X (2019) Developmental origins and oncogenic pathways in malignant brain tumors. Wiley Interdiscip Rev Dev Biol 8(4):1–23
11. Louis DN, Perry A, Wesseling P, Brat DJ, Cree IA, Figarella-Branger D et al (2021) The 2021 WHO classification of tumors of the central nervous system: a summary. Neuro Oncol 23(8):1231–1251
12. Gojo J, Pavelka Z, Zapletalova D, Schmook MT, Mayr L, Madlener S et al (2020) Personalized treatment of H3K27M-mutant pediatric diffuse gliomas provides improved therapeutic opportunities. Front Oncol 9(January):1–14
13. Karremann M, Gielen GH, Hoffmann M, Wiese M, Colditz N, Warmuth-Metz M et al (2018) Diffuse high-grade gliomas with H3 K27M mutations carry a dismal prognosis independent of tumor location. Neuro Oncol 20(1):123–131
14. Buczkowicz P, Bartels U, Bouffet E, Becher O, Hawkins C (2014) Histopathological spectrum of paediatric diffuse intrinsic pontine glioma: diagnostic and therapeutic implications. Acta Neuropathol 128(4):573–581
15. Chen H, Hu W, He H, Yang Y, Wen G, Lv X (2019) Noninvasive assessment of H3 K27M mutational status in diffuse midline gliomas by using apparent diffusion coefficient measurements. Eur J Radiol 114:152–159
16 Schreck KC, Ranjan S, Skorupan N, Bettegowda C, Eberhart CG, Ames HM et al (2019) Incidence and clinicopathologic features of H3 K27M mutations in adults with radiographically-determined midline gliomas. J Neurooncol. 143(1):87–93. https://doi.org/10.1007/s11060-019-03134-x

17. Aboian MS, Solomon DA, Felton E, Mabray MC, Villanueva-Meyer JE, Mueller S et al (2017) Imaging characteristics of pediatric diffuse midline gliomas with histone H3 K27M mutation. Am J Neuroradiol 38(4):795–800
18. Thust SC, Hassanein S, Bisdas S, Rees JH, Hyare H, Maynard JA et al (2018) Apparent diffusion coefficient for molecular subtyping of non-gadolinium-enhancing WHO grade II/III glioma: volumetric segmentation versus two-dimensional region of interest analysis. Eur Radiol 28:3779–3788
19. Lee S, Choi SH, Ryoo I, Yoon TJ, Kim TM, Lee SH et al (2015) Evaluation of the microenvironmental heterogeneity in high-grade gliomas with IDH1/2 gene mutation using histogram analysis of diffusion-weighted imaging and dynamic-susceptibility contrast perfusion imaging. J Neurooncol 121(1):141–150
20. Patterson DM, Padhani AR, Collins DJ (2008) Technology insight: water diffusion MRI - a potential new biomarker of response to cancer therapy. Nat Clin Pract Oncol. 5:220–233
21. Cui Y, Ma L, Chen X, Zhang Z, Jiang H, Lin S (2014) Lower apparent diffusion coefficients indicate distinct prognosis in low-grade and high-grade glioma. J Neurooncol 119:377–385
22. Law M, Young RJ, Babb JS, Peccerelli N, Chheang S, Gruber ML et al (2008) Gliomas: predicting time to progression or survival with cerebral blood volume measurements at dynamic susceptibility-weighted contrast-enhanced perfusion MR imaging. Radiology 247(2):490–498
23. Rossi A, Gandolfo C, Morana G, Severino M, Garrè ML, Cama A (2010) New MR sequences (diffusion, perfusion, spectroscopy) in brain tumours. Pediatr Radiol 40(6):999–1009
24. Xing Z, Yang X, She D, Lin Y, Zhang Y, Cao D (2017) Noninvasive assessment of IDH mutational status in World Health Organization grade II and III astrocytomas using DWI and DSC-PWI combined with conventional MR imaging. Am J Neuroradiol 38(6):1138–1144
25. Yamashita K, Hiwatashi A, Togao O, Kikuchi K, Hatae R, Yoshimoto K et al (2016) MR imaging-based analysis of glioblastoma multiforme: estimation of IDH1 mutation status. Am J Neuroradiol 37(1):58–65
26. Darbar A, Waqas M, Enam SF, Mahmood SD (2018) Use of preoperative apparent diffusion coefficients to predict brain tumor grade. Cureus. 10(3):e2284
27. Murakami R, Hirai T, Sugahara T, Fukuoka H, Toya R, Nishimura S et al (2009) Grading astrocytic tumors by using apparent diffusion coefficient parameters: superiority of a one- versus two-parameter pilot method. Radiology 251(3):838–845
28. Boxerman JL, Schmainda KM, Weisskoff RM (2006) Relative cerebral blood volume maps corrected for contrast agent extravasation significantly correlate with glioma tumor grade, whereas uncorrected maps do not. Am J Neuroradiol 27(4):859–867
29. Saini J, Gupta RK, Kumar M, Singh A, Saha I, Santosh V et al (2019) Comparative evaluation of cerebral gliomas using rCBV measurements during sequential acquisition of T1-perfusion and T2-perfusion MRI. PLoS ONE 14(4):1–14
30. Hu LS, Baxter LC, Smith KA, Feuerstein BG, Karis JP, Eschbacher JM et al (2009) Relative cerebral blood volume values to differentiate high-grade glioma recurrence from posttreatment radiation effect: direct correlation between image-guided tissue histopathology and localized dynamic susceptibility-weighted contrast-enhanced perfusio. Am J Neuroradiol 30(3):552–558
31. Wetzel SG, Cha S, Johnson G, Lee P, Law M, Kasow DL et al (2002) Relative cerebral blood volume measurements in intracranial mass lesions: interobserver and intraobserver reproducibility study. Radiology 224(3):797–803
32. Danchaivijitr N, Waldman AD, Tozer DJ, Benton CE, Caseiras GB, Tofts PS et al (2008) Low-grade gliomas: do changes in rCBV measurements at longitudinal perfusion-weighted MR imaging predict malignant transformation? Radiology 247(1):170–178
33. Mazur MD, Couldwell WT (2011) Investigating a candidate cell of origin for diffuse intrinsic pontine glioma. World Neurosurg. 76:368–373
34. Duchatel RJ, Jackson ER, Alvaro F, Nixon B, Hondermarck H, Dun MD (2019) Signal transduction in diffuse intrinsic pontine glioma. Proteomics. 19:e1800479
35. Piccardo A, Tortora D, Mascelli S, Severino M, Piatelli G, Consales A et al (2019) Advanced MR imaging and 18F-DOPA PET characteristics of H3K27M-mutant and wild-type pediatric diffuse midline gliomas. Eur J Nucl Med Mol Imaging 46(8):1685–1694
36. Yao R, Cheng A, Liu M, Zhang Z, Jin B, Yu H (2021) The diagnostic value of apparent diffusion coefficient and proton magnetic resonance spectroscopy in the grading of pediatric gliomas. J Comput Assist Tomogr 45(2):269–276
37. Lee J, Choi SH, Kim JH, Sohn CH, Lee S, Jeong J (2014) Glioma grading using apparent diffusion coefficient map: application of histogram analysis based on automatic segmentation. NMR Biomed 27(9):1046–1052
38. Chawla S, Kim S, Wang S, Poptani H (2009) Diffusion-weighted imaging in head and neck cancers. Futur Oncol 5(7):959–975